International Journal of Signal Processing, Image Processing and Pattern Recognition
Vol.9, No.11, (2016), pp.283-296
http://dx.doi.org/10.14257/ijsip.2016.9.11.26

Multi-Sensor Image Fusion with Adaptive Guided Image Filtering in Nonsubsampled Contourlet Transform Domain

Zhenbing Zhao[1], Yinping Cai[1*], Yincheng Qi[1] and Ning Liu[1]

[1]North China Electric Power University, School of Electrical and Electronic Engineering, No. 619 Yonghua North Main Street, Baoding, Hebei, 071003, China,
[1]zhaozhenbing@ncepu.edu.cn
[*]ncepu_cyp@126.com

Abstract

Aiming at the problems that the luminance information is not enough and the edge information can not be preserved easily in the process of the image fusion, an effective image fusion method based on nonsubsampled contourlet transform (*NSCT*) *and adaptive guided image filtering is proposed in this paper. Firstly the source images are decomposed by NSCT with multi-scale, multi-direction and shift-invariant properties. The fusion rule of the low-frequency subband coefficients employs the local correlation energy to improve the energy and information of the subband coefficients. To acquire good effects with edge-preserving and noise reduction, the adaptive guided image filtering is introduced to the high-frequency subband coefficients as the fusion rule for the first time, and it can make use of halo-free edge slope enhancement in the fusion process. Finally, the fused image is reconstructed by the inverse NSCT. Experimental results demonstrate that the comprehensive performances of the proposed method are improved in the fusion information, edge and luminance.*

Keywords: *image fusion, NSCT, guided filter, adaptive guided image filtering, local correlation energy*

1. Introduction

With the development of sensor technology, multiple visual sensors replace the single sensor model. The multiple sensors information is often redundant and complementary, and the fusion of multiple sensors information can reduces the overall uncertainty and increase the accuracy. Multi-sensor image fusion has been applied to some areas including remote sensing satellite images processing, visible and infrared images processing, medical images processing and so on. The primary purpose of image fusion is reserving most of the useful information for different images. For this purpose, a large number of image fusion methods have been proposed in literatures. Researchers also gradually improve the quality of the fused image such as sharpness, brightness, edge, and detail. According to different fusion levels of image fusion technology, image fusion can generally be divided into three levels including the pixel level fusion, feature level fusion and decision level fusion [1]. The pixel level fusion has attracted most of the researchers for its low level and high precision, and it can be divided into two categories: the spatial domain and transform domain. The final quality of the pixel fusion effect depends on the choices of the transform and fusion rules.

Nowadays, transform domain fusion algorithms based on multi-scale geometric analysis such as pyramid transform, wavelet transform, contourlet transform (CT), and NSCT have achieved great success. Pyramid decomposition is redundant, no-directional

[*]Corresponding Author

ISSN: 2005-4254 IJSIP

and correlative among the layers, resulting in losing the high frequency information and detail feature of the fused images [2]. Wavelet transform is a non-redundant and multi-directional decomposition, retaining the spectral and spatial information of the image [2]. However, the wavelet base is isotropic and limited by direction description, failing to reflect the high-dimensional contour information of the image. CT is put forward by M. N. Do and has the properties of multi-resolution, localization, directionality and anisotropy [4-5], but its implementation requires down-samplers and up-samplers that cause spectrum aliasing and the pseudo-Gibbs phenomenon [6]. NSCT [7], proposed by A. L. Da Cunha, *etc.,* in 2006, not only inherits all the advantages of CT, but also possesses the shifted invariance. Therefore, NSCT can accurately extract the outline and the detail information of the image and overcome shortcomings arising from other transforms [8]. Based on the advantages of NSCT, it is chosen as the tool of multi-scale transform in this paper.

Another key point of the final fused results is the fusion rules. Well-designed fusion rules for coefficients of multi-scale transform can further enhance the effect of fusion. Through multi-scale transform, the original images are often divided into the high-frequency subband coefficients and the low-frequency subband coefficients. The fusion rules of the low-frequency subband coefficients commonly include average method, weighted average method, the largest area method, *etc.,* [9-10]. For the low-frequency subband coefficients, the average method and weighted average method are easy to be implemented, but the edge information and luminance feature are lost. The fusion rules of the high-frequency subband coefficients include the absolute maximum, the maximum area of energy, the absolute maximum variance, *etc.,* [11-13]. In conclusion, these methods do not consider the variations of the energy and relevancy in a certain region, resulting in low brightness and blurred edges of the fusion image. And the final fusion images of these methods may lose some useful information such as edge information, luminance information and detail information, and at the same time, decrease the contrast of the fusion image. Therefore, it need better fusion rules to improve the existing fusion rules.

The proposed guided image filtering [14] fulfills the requirements of both edge preserving and linear complexity. It has been applied to some fields such as image matting and colorization [15-17]. S. Li [18] applies the guided image filtering to image fusion and achieves good results, but the images are decomposed into base layer and detail layer by average filtering instead of multi-scale transform. At the same time, the guided image filtering does not realize adaptively choosing the parameters that can create halo artifacts in the slope of edges. Based on guided image filtering, C. C. Pham [19] proposes adaptive guided image filtering (AGF) that realizes adaptive filtering, superior sharpness enhancement and noise reduction. In this paper, the thought introducing the AGF to the NSCT domain is first proposed and applied to image fusion.

Based on analysis above, a new and effective image fusion method is proposed in this paper, which combines the local correlation energy and AGF in NSCT domain. The method ensures the multi-scale decomposition of the images, and also combines the latest edge-preserving technology. It can achieve fine fusion effects including distinct edge, high luminance and more detail information.

2. NSCT

In this section, the key ideas and properties of the NSCT will be reviewed briefly. The NSCT has the quality of shift-invariance, multi-scale and multi-direction. It consists of nonsubsampled pyramid (NSP) and nonsubsampled directional filter bank (NSDFB), which ensure the multi-scale and multi-directional decomposition of the NSCT respectively. First of all, the image is decomposed into different scales by NSP. NSP can result in L+1 sub-images, which consists of one low-frequency and L high-frequency

images with the same size as the source image, where L denotes the number of decomposition levels. And then the high-frequency subband image is decomposed by NSDFB and obtained the final subband images at different scales and directions. NSDFB produces 2^J directional sub-images with the same size as the source image by J-level decomposition. The total number of decomposition is given by $1+\sum_{j=1}^{J} 2^{l_j}$, where l_j denotes the number of levels in NSDFB at the jth scale. The structure of NSCT is shown in Figure 1.

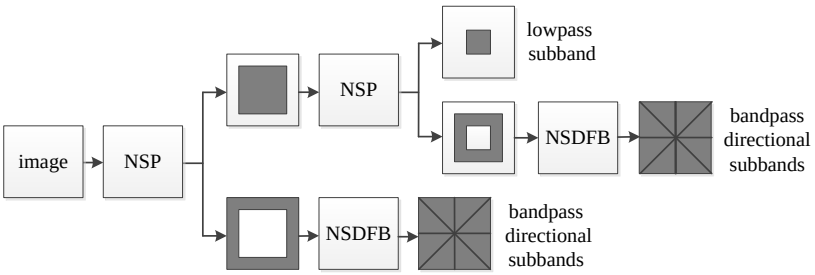

Figure 1. The Structure of NSCT

3. Guided Image Filtering

In [14], the guided image filtering has some good properties. The guided image filtering has good edge-preserving properties as the bilateral filter, and it overcomes the gradient reversal artifacts. The guided image filtering involves a guidance image G, a filtering input image I, and an output image O. The guided filter output at a pixel i is expressed as a weighted average:

$$O_i = \sum_j W_{ij}(G) I_j, \tag{1}$$

where i and j are pixel indexes. The filter kernel W_{ij} is a function of the guidance image G and independent of I, defined as follows:

$$W_{ij}(G) = \frac{1}{|w|^2} \sum_{k:(i,j)\in w_k} \left(1 + \frac{(G_i - \mu_k)(G_j - \mu_k)}{\sigma_k^2 + \varepsilon}\right). \tag{2}$$

Here, w_k is a square window of size $(2r+1)\times(2r+1)$ centered at the pixel k. $|w|$ is the number of pixels in w_k. μ_k and σ_k^2 are the mean and variance of G in w_k. ε is a regularization parameter given by the user.

Compared with the traditional filter kernel function, the guided image filtering kernel function has good edge-preserving and detail enhancement properties. At the same time, the computing time is independent of the filter size. On account of its qualities, the guided image filtering has performed very well in a great variety of applications including image smoothing, enhancement, image matting and dehazing. In this paper, the guided filter is applied to image fusion.

4. The Proposed Method and Its Fusion Rules

4.1. General Framework for the Proposed Method

A general framework of image fusion in NSCT domain is shown in Figure 2. Firstly, the source images (A,B) are decomposed by NSCT to acquire the low-frequency subband images $C_{l_0}^X$ (X=A,B) and high-frequency subband images $H_{l,\theta}^X$ (X=A,B) respectively. $H_{l,\theta}^X$ (X=A,B) represents the high-frequency subband images at level $l\in[1,L]$ in the

orientation θ. Then the local correlation energy is used as the fusion rule of the low-frequency subband images. The AGF is employed as the fusion rule of the high-frequency subband images. Finally, inverse NSCT is applied to the new low and high frequency subband images and the final fusion image is obtained.

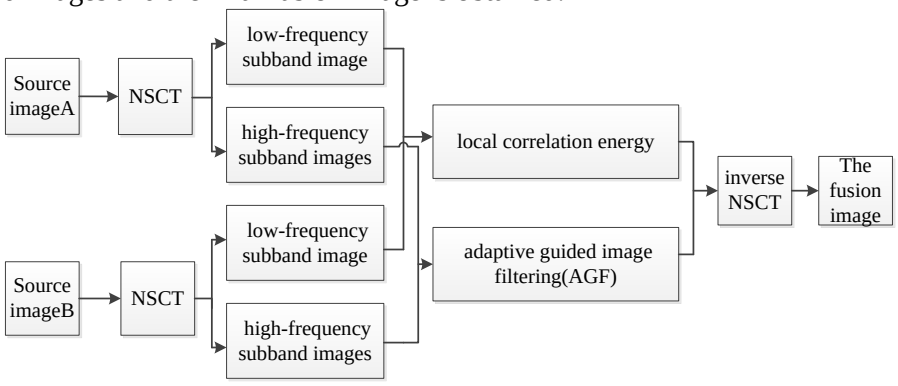

Figure 2. The General Framework of Image Fusion in NSCT Domain

4.2. Low Frequency Fusion Rule

The low-frequency subband images reflect the average characteristics of the source images and determine the outline of the images. And the correlation coefficient of image represents the similarity of two images in each area [20-21]. The local energy of the image represents that how much the amount of energy information contains in the image area. The local energy can be used to guide the choice of low-frequency subband images. The previous methods that choose window randomly, and the proposed method selects window corresponding to the window size of AGF to ensure the consistency between high and low frequency. The decisions of fusion rule based on the local correlation energy can merge information of source images and keep the details of the fused image.

The definition of local correlation coefficient R is

$$R = \frac{\sum_{m=1}^{M}\sum_{n=1}^{N}\left(C_{l_0}^{A}(m,n)-\mu_A\right)\left(C_{l_0}^{B}(m,n)-\mu_B\right)}{\sqrt{\left(\sum_{m=1}^{M}\sum_{n=1}^{N}\left[C_{l_0}^{A}(m,n)-\mu_A\right]^2\right)\left(\sum_{m=1}^{M}\sum_{n=1}^{N}\left[C_{l_0}^{B}(m,n)-\mu_B\right]^2\right)}}. \quad (3)$$

Here, μ_X (X=A,B) is the mean of the low-frequency subband images. $M\times N$ is the size of the area.

The local energy of the image is calculated by (4)

$$E_{l_0}^{X}(m,n) = \frac{1}{MN}\sum_{x=-(M-1)/2}^{(M-1)/2}\sum_{y=-(N-1)/2}^{(N-1)/2}\left(C_{l_0}^{X}(m+x,n+y)\right)^2. \quad (4)$$

The low-frequency subband images are first divided into some $M\times N$ sub-regions. And then the new low-frequency coefficients are calculated by using the local correlation energy according to (5) and (6).

If $R\geq TH$,

$$C_{l_0}^{O}(m,n) = \begin{cases} R\times C_{l_0}^{A}(m,n) + (1-R)\times C_{l_0}^{B}(m,n), & E_{l_0}^{A} \geq E_{l_0}^{B} \\ (1-R)\times C_{l_0}^{A}(m,n) + R\times C_{l_0}^{B}(m,n), & E_{l_0}^{A} < E_{l_0}^{B} \end{cases}, \quad (5)$$

If $R < TH$,

$$C_{l_0}^{O}(m,n) = \begin{cases} C_{l_0}^{A}(m,n), & E_{l_l}^{A} \geq E_{l_0}^{B} \\ C_{l_0}^{B}(m,n), & E_{l_0}^{A} < E_{l_0}^{B} \end{cases}. \quad (6)$$

Here, E^{A}_{l0} and E^{B}_{l0} are local energy of the sources images respectively. *TH* is the threshold of *R*. $C^{O}_{l0}(m,n)$ is the new low-frequency coefficient after fusion.

4.3. High Frequency Fusion Rule

High-frequency subband images represent the detail component of the image, including the edge and texture of the source image, and directly relate to the final fusion effect. In this paper, the AGF as the fusion rules of high frequency subband images is first proposed and applied. It performs halo-free edge slope enhancement and noise reduction simultaneously, and has been implemented by using a fast and exact linear-time algorithm. For high frequency subband images of multi-sensor images, the edge of the images can integrate together without artifact by using AGF. Compared with guided image filtering, the improvement of AGF is the offset ξ_i that is added to the intensity value of center pixel *k* in the kernel weights function of guided image filtering. The new high-frequency coefficients after fusion are calculated by the filter kernel and weighting function of AGF:

$$AGF(G)_i = \sum_j W_{AGF_{ij}}(G) I_j, \quad (7)$$

$$W_{AGF_{ij}}(G^{F}_{l,\theta}) = \frac{1}{|w|^2} \sum_{k:(i,j)\in w_k} \left(1 + \frac{((G_i + \xi_i) - \mu_k)(G_j - \mu_k)}{\sigma_k^2 + \varepsilon}\right). \quad (8)$$

Here, $G_i = H^{A}_{l,\theta}$ and $G_j = H^{B}_{l,\theta}$. $G^{F}_{l,\theta}$ is the new high-frequency coefficients after fusion. ξ_i is the added offset. An offset-choosing strategy is also applied in AGF, in the same manner as described in adaptive bilateral filter [22-23].That is:

$$\xi_i = \begin{cases} MAX(\omega_k) - G_i & \Delta_i > 0 \\ MIN(\omega_k) - G_i & \Delta_i < 0. \\ 0 & \Delta_i = 0 \end{cases} \quad (9)$$

Here the intensity difference is defined by $\Delta_i = G_i - \mu_k$.

After the processing, the new low and high frequency coefficients are acquired. And the final fusion image is obtained by inverse NSCT.

5. Experimental Results and Analysis

5.1. The Experimental Results

In order to verify the effectiveness of the proposed method, it is compared with nine multi-scale transform–based methods, including, ratio pyramid(RAT) [24], Laplacian pyramid(LAP) [25], gradient pyramid(GRP) [26], FSD pyramid(FSDP) [27], DWT [28], contourlet transform based on guided image filtering (CT-GF), nonsubsampled contourlet transform based on guided image filtering (NSCT-GF), nonsubsampled contourlet transform based on bilateral filter (NSCT-BF) and guided image filtering based fusion method(GFF) [18]. The decomposition level of all method is *L*=3. Parameters of fusion methods 1 to 5 are: Burts method for the high-frequency subband images and average method for the low-frequency subband images. And the fusion rules of the high-frequency and low-frequency subband coefficients use guide image filtering of CT-GF and NSCT-

GF. For NSCT-BF, the fusion rules of the high-frequency and low-frequency subband coefficients use bilateral filter and local correlation energy respectively. The GFF uses the method in [18]. This paper selects three sets of multi-sensor images including medical images, infrared and visible images and remote sensing images. The experimental results are presented respectively.

The results of the medical images

As shown in Figure 3, the first set of experiments is the medical images fusion, choosing CT (computed tomography) and MRI (magnetic resonance imaging) images as the source images. It can be seen from the experimental results that the proposed method is the best way combined the information of the source images. The experimental results (c–h) have the phenomenon of low grayscale and blurred edges caused by incomplete decomposition and improper low frequency fusion rules. Compare to the experimental results (c–h), the fusion image of the proposed method does not appear blurred edges due to the shift-invariance of NSCT. And the luminance of the fusion image does not change much, because the local correlation energy algorithm used in the low-frequency subband images fusion can retain the image information. As shown in experimental results (i-k), the edges are kept by using guided image filtering and at the same time the luminance information is preserved. The automatic selection of parameters is realized by using adaptive guided image filtering in the proposed method, so the edge is clear and has no halo artifacts.

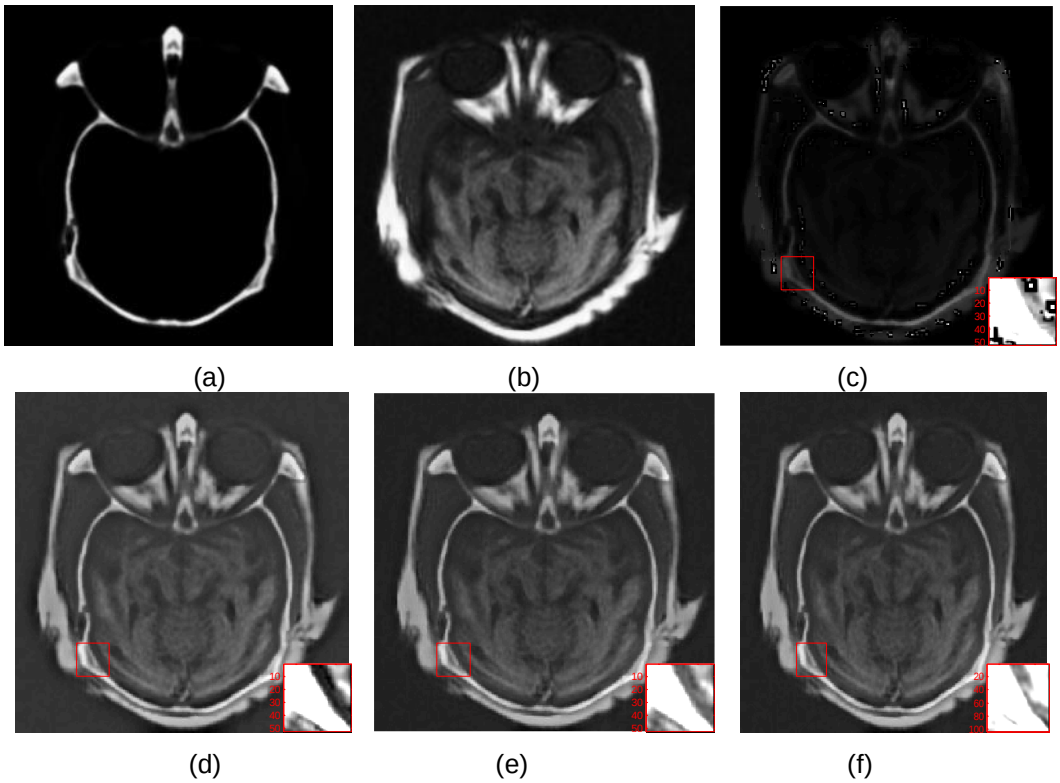

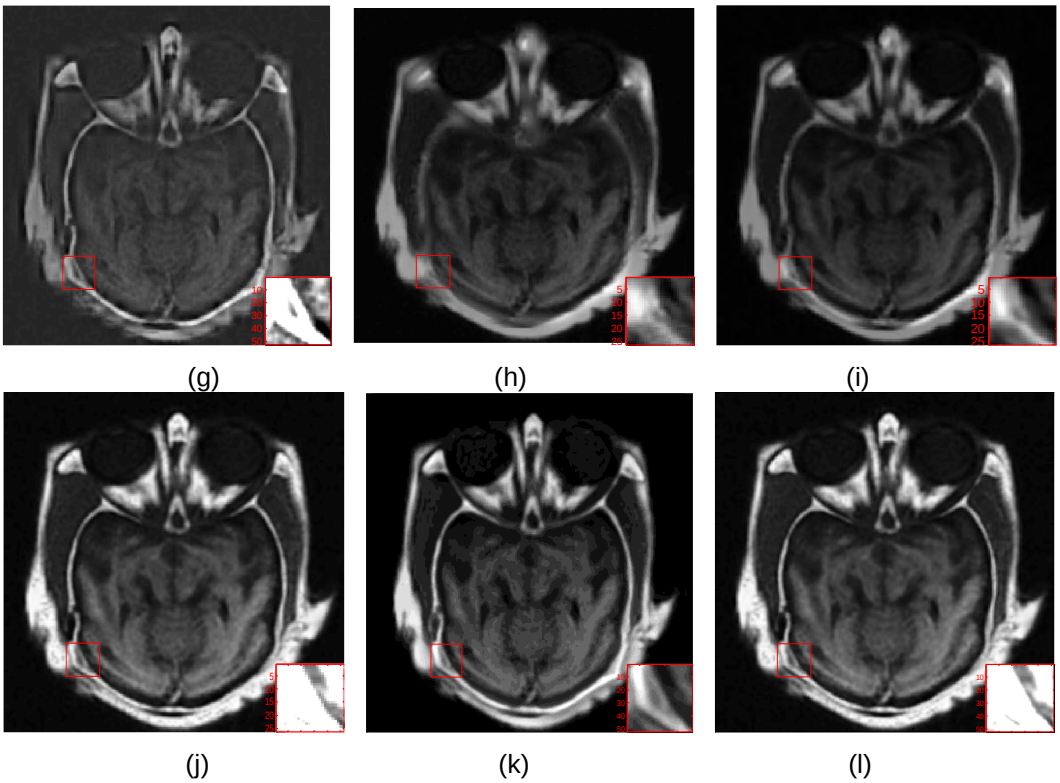

Figure 3. The Experimental Results of the Medical Images. (a) Image A. (b) Image B. (c) RAT. (d) LAP. (e) GRP. (f) FSDP. (g) DWT. (h) CT-GF. (i) NSCT-GF. (j) NSCT-BF. (k) GFF. (l) The Proposed Method.

The results of the infrared and visible images

As shown in Figure 4, the source images are the infrared image and visible image about the nighttime street corner. The proposed method combines the infrared image and visible image information. And the contour of the hang letters and pedestrians are more obvious. At the same time, the luminance and contrast of the fused image in the proposed method is higher than that of other methods.

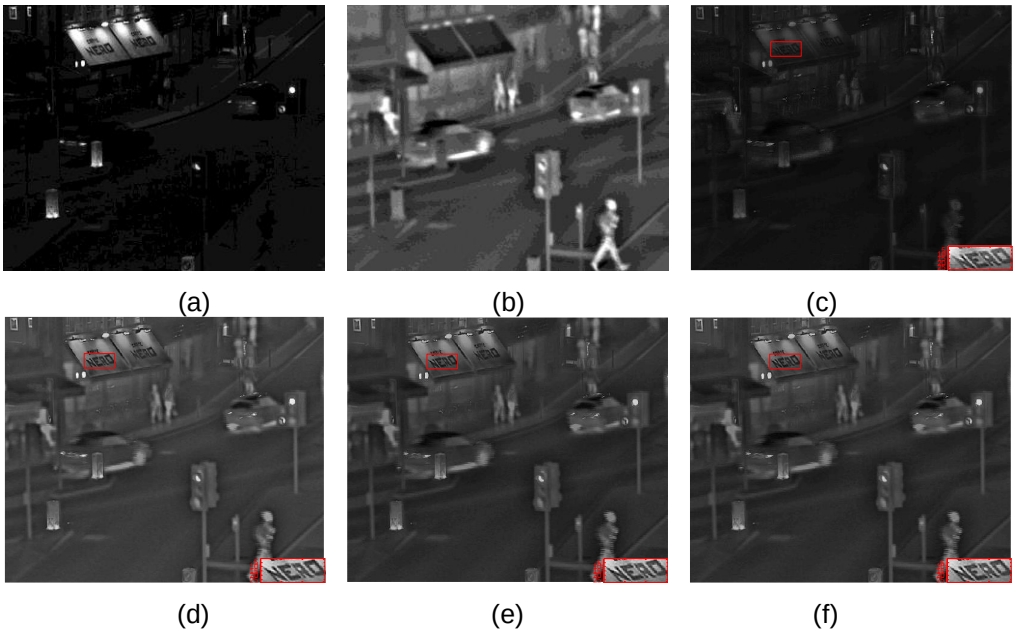

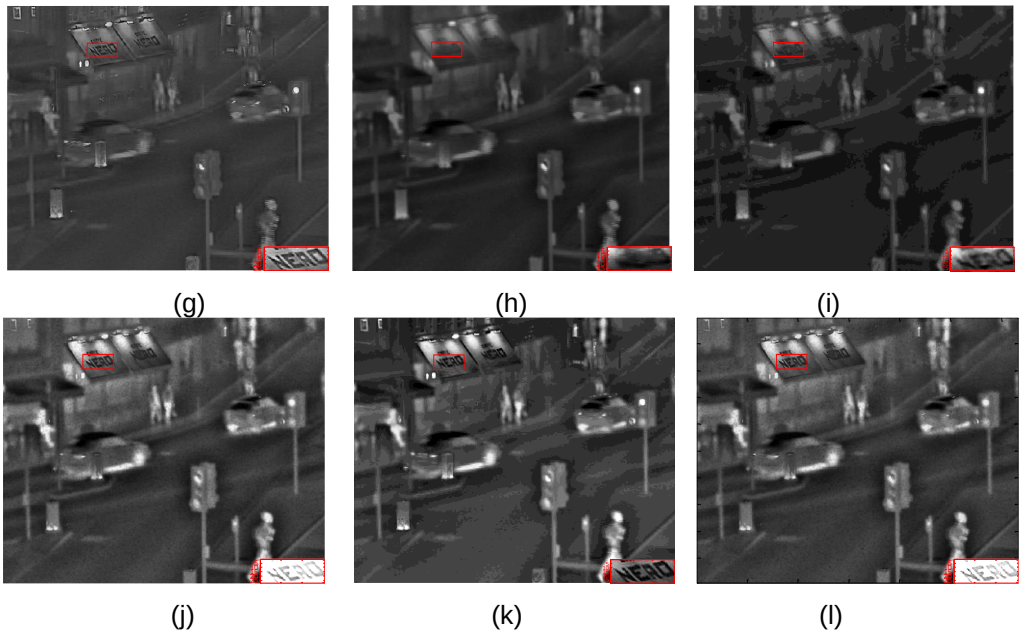

Figure 4. The Experimental Results of the Infrared and Visible Images. (a) Image A. (b) Image B. (c) RAT. (d) LAP. (e) GRP. (f) FSDP. (g) DWT. (h) CT-GF. (i) NSCT-GF. (j) NSCT-BF. (k) GFF. (l) The Proposed Method.

The results of the remote sensing images

As shown in Figure 5, the source images of the third group experiments are remote sensing images. It can be seen from the experimental results that the proposed method makes the source image better together, and not only enriches the source image information, but also preferably reflects the details information. It can preserve the complementary information of different source images such as the edge of the round object. Meanwhile, the brightness and edge of the image fusion results also has a good performance.

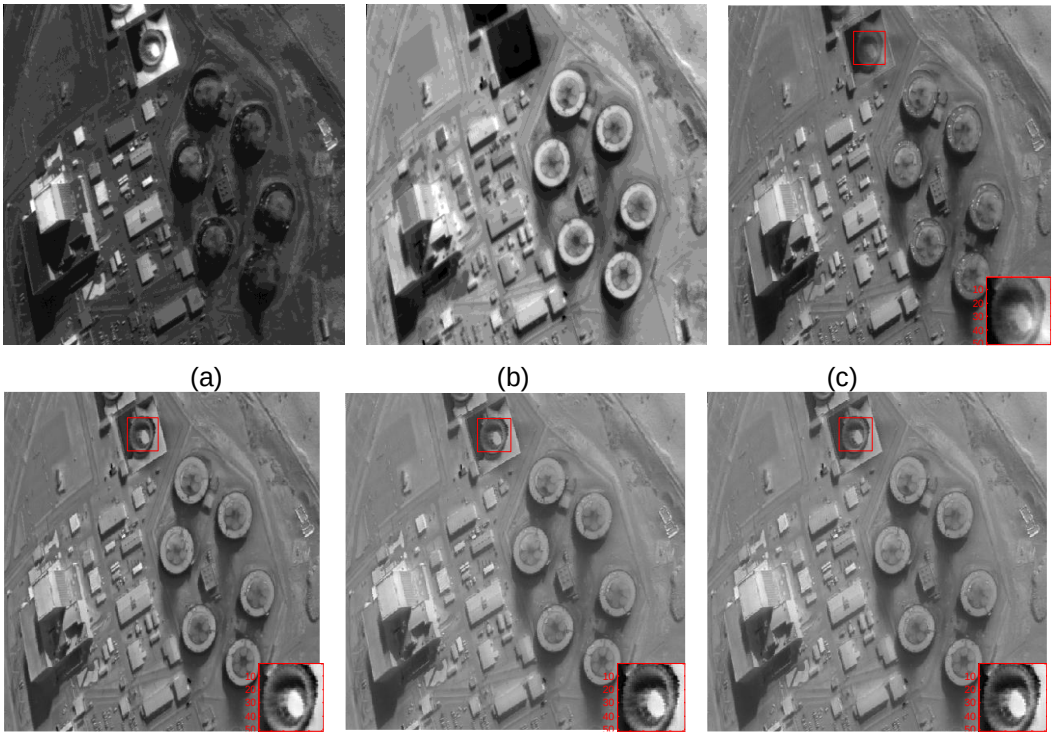

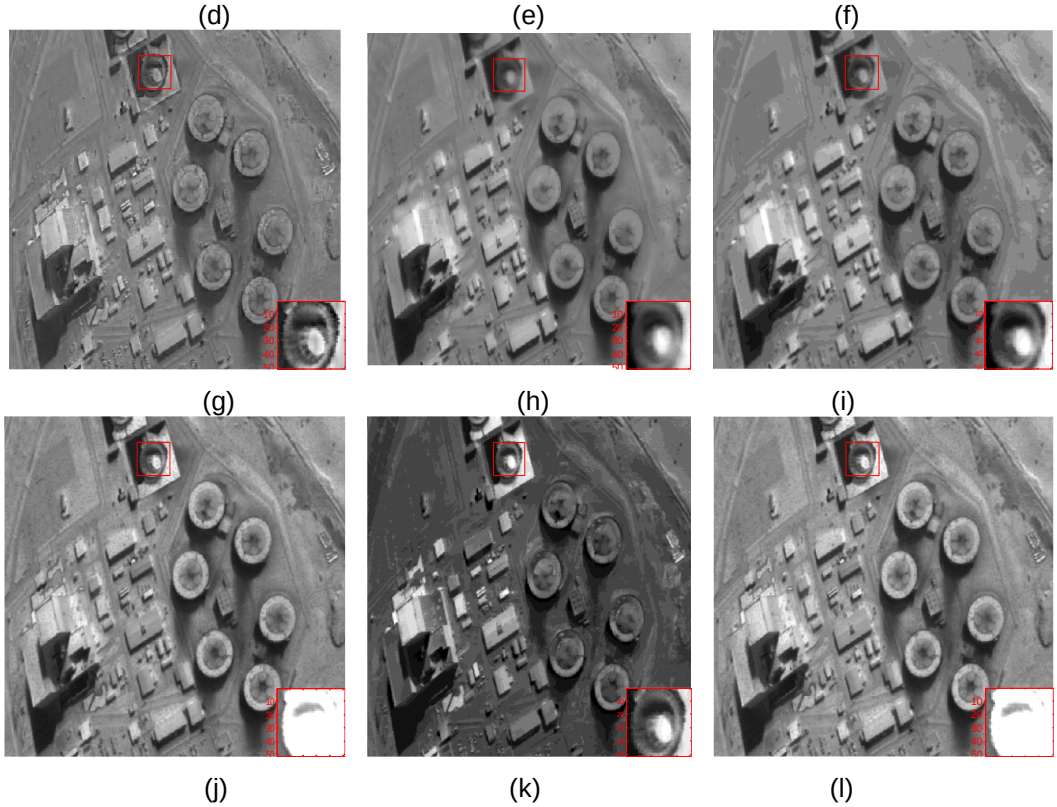

Figure 5. The Experimental Results of the Remote Sensing Images. (a) Image A. (b) Image B. (c) RAT. (d) LAP. (e) GRP. (f) FSDP. (g) DWT. (h) CT-GF. (i) NSCT-GF. (j) NSCT-BF. (k) GFF. (l) The Proposed Method.

5.2. The Evaluation Indexes

To estimate the fusion performances of different methods objectively, five evaluation indexes are employed, *i.e.*, mean (Q_μ), entropy (Q_E), the edge intensity (Q_{EI}), the standard deviation(Q_{SD}), and mutual information (Q_{MI}) [29].

1) Mean (Q_μ): The mean of the image is the arithmetic average of all pixels luminance, stands for the average luminance and reflectance ratio of the image. The greater the mean of the results is, the more brightness information inherited from the source image is.

$$Q_\mu = \frac{1}{M \times N} \sum_{x=1}^{M} \sum_{y=1}^{N} f(x, y), \tag{10}$$

where, M and N are the size of the image, and $f(x,y)$ is the value of gray.

2) The information entropy (Q_E): The entropy represents the richness of the image contained information. A small information entropy value corresponds to a narrow distribution function, which means that the uncertainty of the related random variable is small.

$$Q_E = -\sum_{i=0}^{L-1} P_i \log_2 P_i, \tag{11}$$

here, P_i represents the probability of the pixels.

3) The edge intensity (Q_{EI}): Since edge information is very important for human perception, the metric is developed based on this information transferred from the source images to the fused image.

$$Q_{EI} = \frac{1}{M \times N} \sum_{x=1}^{M} \sum_{y=1}^{N} \sqrt{f_x^2 + f_y^2}, \tag{12}$$

here, f_x and f_y are got by "soble" filtering algorithm.

4) The standard deviation(Q_{SD}): Human perception is very sensitive to intensity changes and higher intensity variations in an image reveal large Q_{SD}. So the Q_{SD} matrix can determine the dynamic range of gray level change. The bigger Q_{SD} is, the greater the contrast of fused images is, and the better the clarity is.

$$Q_{SD} = \left[\frac{1}{M \times N} \sum_{x=1}^{M} \sum_{y=1}^{N} \left(f(x, y) - M \right)^2 \right]^{\frac{1}{2}}, \tag{13}$$

where M is the average grey level of the fused image.

5) The mutual information (Q_{MI}): The mutual information is an important and fundamental concept of information theory. Intuitively, mutual information measures the information that image A and image B share. It measures how much these variables reduce uncertainty about the other. Q_{MI} is applied to measure the fusion image how much information inherited from the source images. And the larger of the value is, the better of the fusion results is.

$$Q_{MI} = \sum_{i=0}^{L-1} \sum_{j=0}^{L-1} \sum_{k=0}^{L-1} P_{ABF}(i, j, k) \log_2 \frac{P_{ABF}(i, j, k)}{P_{AB}(i, j) P_F(k)}, \tag{14}$$

where, $P_{ABF}(i,j,k)$ is the grayscale distribution between the fusion image and the source images. And $P_{AB}(i,j)$ is the grayscale distribution between the two source images.

The data statistics of the above three groups of experiments are in the following tables.

Table 1. The Evaluation Indexes of the Medical Images

	Q_μ	Q_E	Q_{EI}	Q_{SD}	Q_{MI}
RAT	35.722	4.186	69.393	47.429	2.547
LAP	34.307	4.294	70.802	49.775	1.698
GRP	33.018	4.266	49.900	37.690	2.002
FSDP	33.183	4.270	50.193	38.039	1.975
DWT	32.088	4.308	64.529	40.230	1.548
CT-GF	32.082	4.114	31.671	32.562	3.161
NSCT-GF	32.082	4.086	35.252	33.846	2.909
NSCT-BF	58.024	4.650	70.255	59.391	3.097
GFF	50.734	*4.714*	69.073	55.477	2.315
Proposed method	***58.024***	**4.659**	***70.851***	***59.433***	***3.559***

Table 2. The Evaluation Indexes of the Infrared Image and Visible Image

	Q_μ	Q_E	Q_{EI}	Q_{SD}	Q_{MI}
RAT	51.496	4.045	26.837	21.407	3.136
LAP	52.035	4.323	34.708	27.180	5.584
GRP	51.957	4.135	25.425	21.934	6.800
FSDP	51.969	4.137	25.560	21.971	6.765
DWT	51.899	4.171	31.637	23.244	5.374
CT-GF	51.904	4.093	16.187	19.975	8.593
NSCT-GF	51.902	4.091	16.270	20.266	7.508
NSCT-BF	81.054	4.654	36.170	34.234	*11.161*
GFF	70.601	4.526	34.441	32.341	6.290
Proposed method	***81.054***	***4.657***	***36.853***	***34.313***	**11.054**

Table 3. The Evaluation Indexes of the Remote Sensing Images

	Q_μ	Q_E	Q_{EI}	Q_{SD}	Q_{MI}
RAT	100.68	4.632	40.078	29.818	1.059
LAP	101.94	4.881	57.732	36.410	3.383
GRP	101.43	4.675	41.271	29.999	3.309
FSDP	101.51	4.680	41.765	30.105	3.280
DWT	101.13	4.752	55.314	32.524	2.419
CT-GF	101.13	4.603	31.576	29.227	4.105
NSCT-GF	101.13	4.611	31.278	29.382	3.461
NSCT-BF	133.23	5.026	58.658	41.522	*8.996*
GFF	82.96	4.705	47.872	34.172	2.986
Proposed method	***133.24***	***5.030***	***59.792***	***41.624***	**8.649**

In those tables, the italics numbers represent the maximum in those methods and the bold numbers correspond to the value of the proposed method. It can be seen from the tables that the proposed method has an advantage of Q_μ which means make great progress in terms of luminance. The proposed method precedes other method in the index of Q_E. It is implying that the fusion results of the proposed method contain more fusion information than that of other methods. The Q_{EI} of the proposed method is maximum. It means the edge preservation effect of the fused image is the best. Although the proposed method is not all maximal in Q_{MI}, the experimental results are better than other methods from the visual effects. Five quality metrics should be considered together to evaluate the real fusion performance.

6. Conclusions

In this paper, a fusion method, which combines the local correlation energy and adaptive guided image filtering, is proposed to solve the defects of image fusion algorithms in NSCT domain. This method has been examined with multi-sensor images in different instrument modalities such as medical image, infrared and visible images, and remote sensing images. From experiments, it can be seen that the proposed method performs better in most cases, and not only maintains the luminance of the image but also retains the edge and detail information of image without halo artifacts. And its performances have been evaluated on the basis of the quantitative criteria. This method can be applied in the processing field of medical diagnosis and target localization. Furthermore, the proposed method is simple in implementation operation.

Acknowledgments

This work was supported in part by the National Natural Science Foundation of China under grant number 61401154 and by the Fundamental Research Funds for the Central Universities under grant number 2015ZD20.

References

[1] O. Prakash, A. Kumar and A. Khare, “Pixel-level Image Fusion Scheme Based on Steerable Pyramid Wavelet Transform Using Absolute Maximum Selection Fusion Rule”, Proceedings of International Conference on Issues and Challenges in Intelligent Computing Techniques, Ghaziabad, **(2014)** February 7-8.

[2] Y. F. Zheng, “Multi-scale Fusion Algorithm Comparisons: Pyramid, DWT and Iterative DWT”, Proceedings of 12th International Conference on Information Fusion, Seattle, WA, **(2009)** July 6-9.

[3] H. J. Wei, M. Viallon, B. M. A. Delattre, K. Moulin, F. Yang, P. Croisille and Y. Zhu, “Free- Breathing Diffusion Tensor Imaging and Tractography of The Human Heart in Healthy Volunteers Using Wavelet-based Iimage Fusion”, IEEE Trans. Medical Imaging, vol. 34, no. 1, **(2015)**, pp. 306-316.

[4] M. N. Do and M. Vetterli, "Contourlets", Studies in Computational Mathematics, vol. 10, **(2003)**, pp. 83-10.
[5] M. N. Do and M. Vetterli, "The Contourlet Transform: An Efficient Directional Multiresolution Image Representation", IEEE Trans. Image Processing, vol. 14, no. 12, **(2005)**, pp. 2091-2106.
[6] G. Bhatnagar, Q. M .J. Wu and Z. Liu, "Directive Contrast Based Multimodal Medical Image Fusion in NSCT Domian", IEEE Trans. Multimedia, vol. 15, no. 5, **(2013)**, pp. 1014-1024.
[7] A. L. Da Cunha, J. Zhou and M. N. Do, "The Nonsubsampled Contourlet Transform: Theory, Design, and Applications", IEEE Trans. Image Processing, vol. 15, no. 10, **(2006)**, pp. 3089-3101.
[8] W. W. Kong, Y. J. Lei, Y. Lei and S. Lu, "Image Fusion Technique Based on Non-subsampled Contourlet Transform and Adaptive Unit-fast-linking Pulse-coupled Neural Network", IET Image Processing, vol. 5, no. 2, **(2011)**, pp. 113-121.
[9] Q. Miao, J. Lou and P. Xu, "Image Fusion Based on NSCT and Bandelet Transform", IEEE International Conference on Computational Intelligence and Security, Guangzhou, China, **(2012)** November 17-18.
[10] D. E. Nirmala, R. K. Vignesh and V. Vaidehi, "Fusion of Multisensory Images Using Nonsubsampled Contourlet Transform and Fuzzy Logic", IEEE International Conference on Fuzzy Systems, Hyderabad, **(2013)** July 7-10.
[11] F. Zhao and Z. Tao, "The Infrared and Visible Images Fusion Based on NSCT", Electronics Optics & Control, vol. 20, no. 9, **(2013)**, pp. 29-33.
[12] X. Sun, J. P. Du, Q. P. Li, X. Y. Li, L. Xu and Y. W. Li, "Improved Energy Contrast Image Fusion Based on Bonsubsampled Contourlet Transform", IEEE International Conference on Industrial Electronics and Applications, Melbourne, VIC, **(2013)** June 19-21.
[13] V. Bhateja, H. Patel, A. Krishn, A. Sahu and A. Lay-Ekuakille, "Multimodal Medical Image Sensor Fusion Framework Using Cascade of Wavelet and Contourlet Transform Domains", IEEE Trans. Sensors Journal, vol. 15, no. 12, **(2015)**, pp. 6783-6790.
[14] K. He, J. Sun and X. Tang, "Guided Image Filtering", IEEE Trans. Pattern Analysis and Machine Intelligence, vol. 35, no. 6, **(2013)**, pp. 1397-1409.
[15] S. Fang, J. R. Yang, Y. Cao, P. F. Wu and R. Z. Rao, "Local Multiscale Retinex Algorithm of Image Guided Filter", Journal of Image and Graphics, vol. 17, no. 7, **(2012)**, pp. 748-755.
[16] C. C. Pham and J. W. Jeon, "Restricted Guided Filter with SURE-LET-Based Parameter Optimization", IEEE International Conference on Image Processing, Orlando, FL, **(2012)** September 30-October 3.
[17] A. Hosni, M. Bleyer and C. Rhemann, "Real-time Local Stereo Matching Using Guided Image Filtering", IEEE International Conference on Multimedia and Expo, Barcelona, **(2011)** July 11-15.
[18] S. Li, X. Kang and J. Hu, "Image Fusion with Guided Filtering", IEEE Trans. Image Processing, vol. 22, no. 7, **(2013)**, pp. 2864-2875.
[19] C. C. Pham, S. V. U. Ha and J. W. Jeon, "Adaptive Guided Image Filtering for Sharpness Enhancement and Noise Reduction", International Conference on Pacific-Rim Symposium on Image and Video Technology, Gwangju, South Korea, **(2011)** November 20-23.
[20] Z. Cao, "A New Image Fusion Algorithm Based on Region Features of Wavelet", Computer Engineering and Applications, vol. 47, no. 26, **(2011)**, pp. 213- 215.
[21] L. Yan and X. Ren, "Image Fusion Algorithm Application of Correlation Coefficient in Wavelet Transform Domain", Computer Engineering and Science, vol. 33, no. 11, **(2011)**, pp. 103-107.
[22] B. Zhang and J. P. Allebach, "Adaptive Bilateral Filter for Sharpness Enhancement and Noise Removal", IEEE Trans. Image Processing, vol. 17, **(2008)**, pp. 664-678.
[23] X. Chen, Y. P. Zheng, J. Y. Guo, Z. Zhu, S. C. Chan and Z. Zhang, "Sonomyographic Responses During Voluntary Isometric Ramp Contraction of The Human Rectus Femoris Muscle", Eur J Appl Physiol, vol. 112, **(2012)**, pp. 2603-2614.
[24] X. M. Zhang and H. Q. Han, "Image Fusion of Multiscale Contrast Pyramid-based Vision Feature and Its Performance Evaluation", Journal of Xi'an Jiaotong University, vol. 38, no. 4, **(2004)**, pp. 380-383.
[25] P. Burt and E. Adelson, "Research on Image Fusion Algorithm Based on Laplacian Pyramid Transform", Laser and Infrared,vol. 391, no. 4, **(2009)**, pp. 440-442.
[26] J. L. Li, J. C. Yu and S. L. Sun, "Study of Image Fusion Based on Gradient Pyramid Algorithm", Science Technology and Engineering, vol. 7, no. 22, **(2007)**, pp. 5819-5822.
[27] P. Sajda, C. Spence and J. Pearson, "Learning Contextual Relationships in Mammograms Using A Hierarchical Pyramid Neural Network", IEEE Trans. Medical Imaging, vol. 21, no. 3, **(2002)**, pp. 239-250.
[28] H. H. Wang, B. S. Peng and W. Wu, "A Fusion Algorithm of Remote Image Based on Discrete Wavlet Packet", IEEE International Conference on Machine learning and Cybernetics, **(2003)** November 2-5.
[29] A. Abd-el-Kader, H. El-Din Moustafa and S. Rehan, "Performance Measures for Image Fusion Based on Wavelet Transform and Curvelet Transform", Natinanl Radio Science Conference, Cairo, **(2011)** April 26-28.

Authors

Zhenbing Zhao, got his B.S. degree in 2002, M.S. degree in 2005 and PhD in 2009 from North China Electric Power University. Now he is an associate professor in School of Electrical and Electronic Engineering, North China Electric Power University. His main research field is intelligent detection of electrical equipment and image processing.

Yinping Cai, received her B.S. degree in 2013 from HEBEI University, Baoding, Hebei, China. Now she is a master student in School of Electrical and Electronic Engineering, North China Electric Power University. Her main research field is image fusion.

Yincheng Qi, received his B.S. degree in 1990, M.S. degree in 1998 and Ph.D. in 2009 from North China Electric Power University, Baoding, Hebei. Now he is a professor in School of Electrical and Electronic Engineering, North China Electric Power University. His main research field is electric power system communication and information processing.

Ning Liu, received her B.S. degree in 2013 from North China Electric Power University, Baoding, Hebei. Now she is a master student in School of Electrical and Electronic Engineering, North China Electric Power University. Her main research field is condition detection of insulator and image recognition.

